Nuclear Instruments and Methods 198 (1982) 233–241
North-Holland Publishing Company

A HIGH DENSITY PROPORTIONAL WIRE CALORIMETER *

T. LUDLAM, R. BELLAZZINI **, D. KRAUS + and J. RENARDY + +
Brookhaven National Laboratory, Upton, N.Y. 11973, U.S.A.

Received 7 December 1981

We describe a total absorption calorimeter consisting of an iron structure penetrated by a fine-grain pattern of small proportional tubes, with a net density ~90% that of pure iron. Designed to be incorporated into the poles of a spectrometer magnet, the device offers a means of constructing highly segmented calorimeters with excellent space resolution as well as good energy resolution. The response of a test module to electron beams is described. A detailed comparison is made with Monte Carlo simulations of electromagnetic showers, which are then used to predict the behavior for a range of sampling geometries.

1. Introduction

The role of calorimeters in large detector systems for colliding beam experiments inevitably leads to the requirements of large solid angle coverage and a finely segmented distribution of sampling elements within the absorber volume. Hence, considerable attention has been given to the development of gas sampling calorimeters as a means of achieving highly segmented devices at relatively low cost.

In an earlier paper [1] we reported on the construction and first tests of an iron calorimeter in which the sampling elements consist of an array of small holes penetrating the iron, each acting as a gas proportional tube, such that 90% of the calorimeter volume is occupied by iron. Our aim was to investigate the technique as a means for instrumenting the pole tips of a spectrometer magnet as active calorimeter elements with a device having very nearly the magnetic properties of pure iron while still maintaining a reasonable energy resolution. We found that acceptable energy resolution can be achieved for the sparse sampling volumes of interest, and that the high net density of the device (which limits the lateral shower development), coupled with a fine-grain array of sampling wires can be exploited to give excellent space resolution, separation of nearby showers and good discrimination between electromagnetic and hadronic showers.

In the present paper we give the results of further test measurements, including the response as a function of incident beam angle, and compare the measured results with a Monte Carlo simulation of electromagnetic showers in the calorimeter. The agreement between the calculated and measured response is quite good, and the calculated results are used to investigate the origin of the fluctuations which govern the energy resolution of this type of calorimeter.

We imagine that high density calorimeter structures – i.e. structures with individual sampling channels penetrating bulk absorber material – as opposed to multiwire planes sandwiched between sheets of absorber material could profitably find applications beyond the instrumentation of flux-carrying magnet iron. In such cases the choice of sampling geometry will be guided by different optimization criteria than those which led to the design of our test module. Thus, in the final section of the paper we use the Monte Carlo calculation to extrapolate our test measurements and parameterize the behavior of such devices in terms of the number and size of individual sampling elements.

2. The calorimeter and test set-up

The calorimeter assembly is illustrated in fig. 1. It consists of a stack of iron plates, 20×20 cm^2, some of which have a row of slots machined on both sides to form the sampling volume. In the assembled stack the slotted plates are interleaved with blank plates, and each of the slots is instrumented as a gas proportional counter with a 12.5 μm diameter wire. The total number of wires in the test module is 720. The active gas is argon/methane in the volume ratio 90/10. The gas was flowed through the device at atmospheric pressure. The total thickness of iron seen by a beam incident along the z axis is 20 radiation lengths.

The sampling geometry is shown in detail in fig. 2a. Each of the slotted plates is 7 mm thick and each slot is

* Work performed under the auspices of the U.S. Department of Energy.
** Permanent address: University of Pisa, Italy.
+ Permanent address: University of Pittsburgh, U.S.A.
+ + Permanent address: CEN, Saclay, France.

0167-5087/82/0000–0000/$02.75

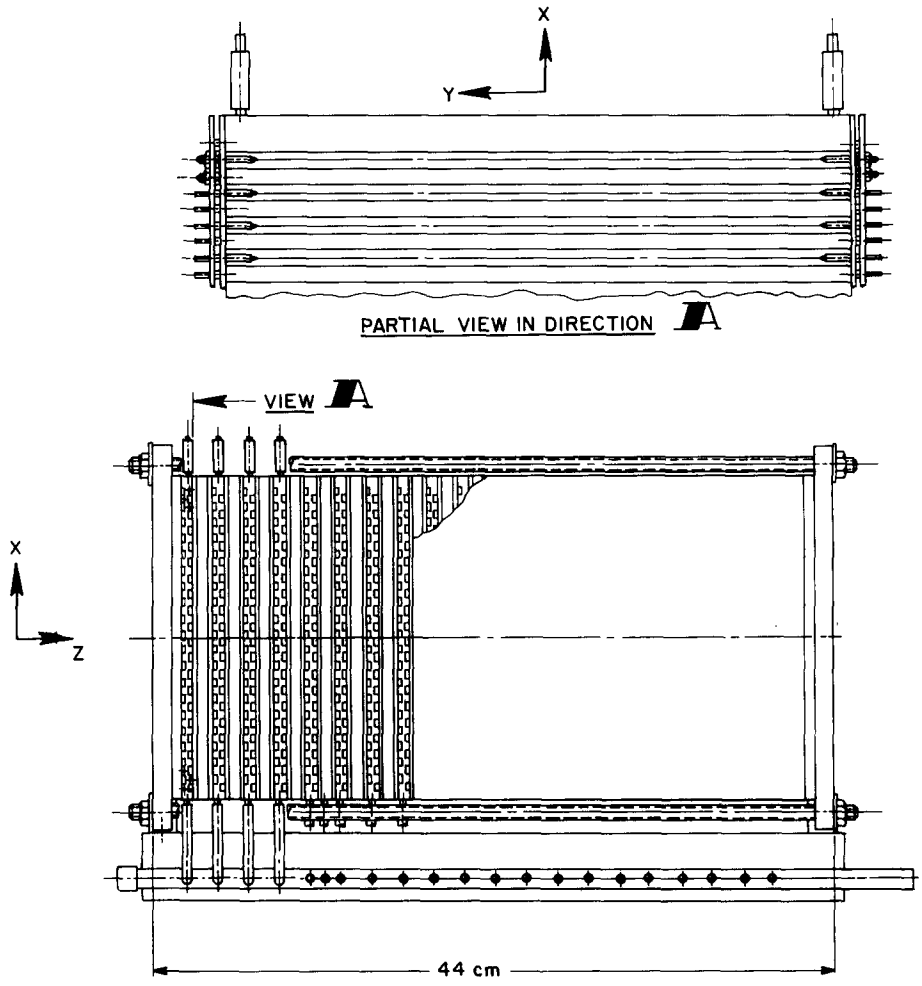

Fig. 1. Assembly drawing of the calorimeter test module. The cross-sectional ($x-y$) view is 2× scale.

2 mm deep by 5 mm wide. The slots are on a 10 mm pitch on either side of the active plates, with the front and back patterns off-set so that a line along the beam direction intersects one slot in each plate. With this geometry the sampling volume is 10% of the total calorimeter volume. The net density of the calorimeter is 7.1 g/cm^3.

The calorimeter was exposed to a Cherenkov-tagged negative beam at the Brookhaven AGS, with data taken at various momentum settings up to 8 GeV/c. (The maximum momentum for electrons was 6 GeV/c.) The device was rotated about an axis through the y–z plane in order to measure its response as a function of the angle of incidence, θ, as illustrated in fig. 2b. The beam size was defined by a scintillator hodoscope 1″ wide in the vertical (x) direction, with seven 1/2″ segments in the horizontal (y) direction.

For the tests described here the readout was configured as follows: Each of the active plates has two layers of wires (front and back) with 18 wires in each layer. The central 6 wires in each layer were separately read out while the signals in each of the outer groups of 6 were summed and presented to a single readout channel. Thus, all wires within ±3 cm of the beam axis (where most of the shower energy is deposited) were readout individually. There were, in all, 264 readout channels.

The calorimeter assembly incorporated a fixed capacitor on each wire through which a known charge could be injected onto the wire with a pulser. Data with the pulser were recorded at frequent intervals during the test runs and used for off-line calibration.

Each readout channel consisted of a charge sensitive preamplifier followed by a bipolar delay line filter with 300 ns shaping time. The pulse heights were digitized with Ortec AD811S ADC units having 11 bits resolution. The equivalent noise charge at the output of our shaping amplifier was measured to be $\sim 3 \times 10^4$ elec-

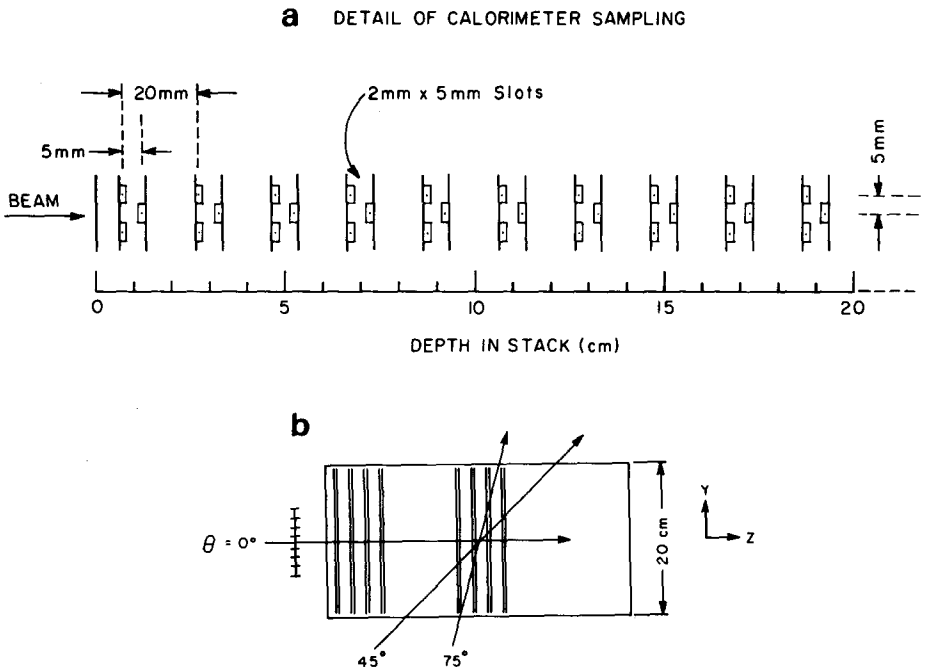

Fig. 2. (a) Layout of sampling slots as a function of depth in the iron structure. Only the first half of the total depth is shown. (b) Plan view defining the angle of beam incidence, θ. The beam-defining hodoscope is indicated at $\theta = 0°$; in practice the calorimeter was rotated through angles θ with respect to the fixed beam direction. The $y-z$ projections of some of the sampling slots are shown.

trons rms. The proportional wires were operated at 1050 V, giving an avalanche gain of $\sim 4 \times 10^4$ in a gas mixture of 90% argon/10% methane at atmospheric pressure. This rather high gain was found necessary for good energy resolution, and can be attributed to the less than ideal charge collection properties of the rectangular slot cross section (see ref. 1).

As an aid in interpreting the results of these tests, and in the hope of being able to use the measurements to predict the response of other sampling geometries, we have implemented a Monte Carlo simulation with which to compare the test data. The EGS routine [2] is used to generate showers in the iron absorber, and the energy loss of shower electrons passing through the sampling gas is modelled in the manner described by Fischer [3]: Each shower electron traversing a gap produces a number of ionization electrons which is determined by the (energy dependent) dE/dx of the shower electron, its path length in the gap, and the mean energy per ion pair in the gas. The total number of ionization electrons, summed over all gaps, is the calculated response of the calorimeter.

Pulse height spectra for 4 GeV/c muons traversing the calorimeter at $\theta = 0°$ are shown in fig. 3, where fig. 3a is the result from the Monte Carlo calculation and fig. 3b shows measurements made in the test beam. For the data the pulse height is shown in terms of ADC counts, after calibration, and can be directly compared

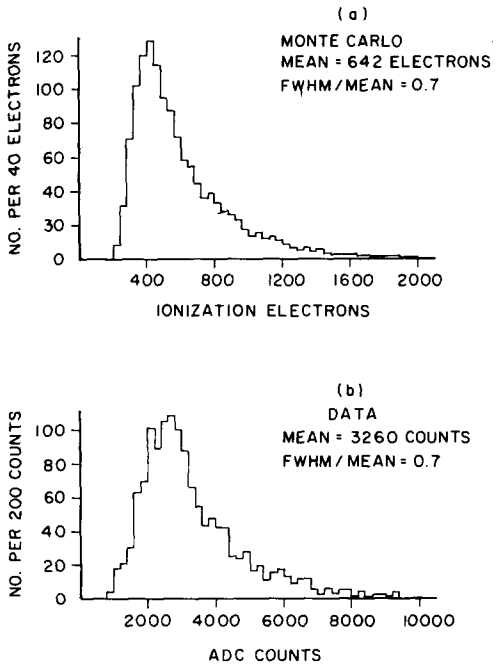

Fig. 3. Pulse height spectra for 4 GeV/c muons traversing the calorimeter at $\theta = 0°$. (a) From the Monte Carlo calculation. (b) Measured data.

with subsequent presentations of the data in this paper. The Monte Carlo result is shown as a function of the number of ionization electrons. The agreement in the shapes of the two distributions is very good, and the ratio of the means gives an absolute calibration factor of 5.0 ADC counts per ionization electron (5.2 eV/ADC count). We find the same factor when comparing data and Monte Carlo calculations for electron showers.

3. Shower measurements with incident electrons

The results for a 4 GeV electron beam, incident at 0°, are shown in fig. 4. The initial Monte Carlo result (fig. 4b) is broader than the data (fig. 4a), with a small but significant tail toward high pulse heights which does not appear in the data. These discrepancies are found to result from occasional very large pulse heights in the Landau tail of the single-track spectrum produced by the Monte Carlo routine. Such fluctuations are suppressed in the data by saturation effects: The response of a single proportional wire gap becomes nonlinear for very large pulse heights as a result of intrinsic saturation (positive ion shielding) and is limited by the finite dynamic range of the readout electronics. These pulse height limiting effects have been studied by illuminating a single wire with radioactive sources over a range of avalanche gains, and are approximated by the function shown in fig. 4d. The circled point in this figure indicates the mean energy deposit per struck gap for a 4 GeV electron shower at 0° incidence. When this curve is folded into the Monte Carlo calculation the result, as shown in fig. 4c, is in good agreement with the width and shape of the measured spectrum.

The fact that the energy resolution of the calorimeter is improved somewhat by single-channel saturation properties gives rise to a concern for the linearity of the device in the total energy measurement. For the range of energies studied here (up to 6 GeV for electron showers) there is no evidence for a nonlinear response due to saturation. Our Monte Carlo simulations indicate that observable deviations from linearity should set in at electron beam energies $\gtrsim 8$ GeV for the operating conditions of these tests. This is a clear motivation for operating a gas sampling calorimeter at the lowest practicable avalanche gain.

Statistical fluctuations in the sampled energy (sampling fluctuations) are measured directly in these tests by treating the calorimeter as two independent interleaved stacks and summing separately for each shower the pulse heights in even-numbered plates (E_a) and odd-numbered plates (E_b). The sum $E_T = E_a + E_b$ measures the total energy deposit, while the difference $E_D = E_a - E_b$ measures the sampling fluctuations. The distribution E_D for 4 GeV electrons at $\theta = 0°$ is shown in fig. 5 for both the data and the Monte Carlo samples. The sampling fluctuations are well fit by a Gaussian distribution. For these electromagnetic showers the energy resolution is determined by the sampling fluctuations.

The mean total pulse height, $\langle E_T \rangle$, and the rms resolution width, σ, for electron showers are shown in figs. 6 and 7 as functions of beam energy and the angle of incidence with respect to the calorimeter axis in the y–z plane. The dashed curves in fig. 6 show the calculated response of the calorimeter assuming it were large enough to fully contain all showers. In fact, for angles $\theta \gtrsim 30°$ the test module was not capable of full containment (see fig. 2a), and so the data points fall below these curves at the higher energies and angles. Nonetheless we assume that the resolution width is accurately determined in all cases by the measured sampling fluctuations, and the points plotted in fig. 7 were obtained in this way.

The dashed curves in fig. 7 are fits to the measured resolution widths of the form

$$\sigma(E,\theta) = \sigma_0(\theta)\sqrt{E}\,. \tag{1}$$

This relation describes the data well, and is in accord with the Monte Carlo calculations. The results obtained for $\sigma_0(\theta)$ are listed in table 1. The measured resolution of the calorimeter for incident electrons of energy E

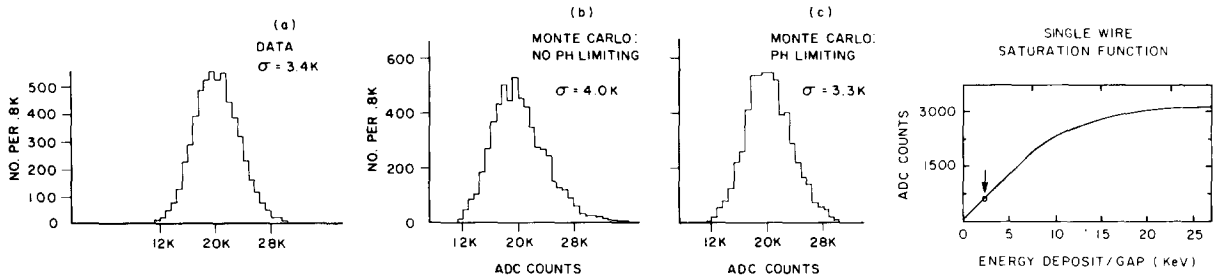

Fig. 4. 4 GeV electrons incident at $\theta = 0°$ (ADC counts in thousands): (a) Measured total pulse height. (b) Calculated response with no saturation effects. (c) Calculated result after imposing the single-wire saturation function shown in (d).

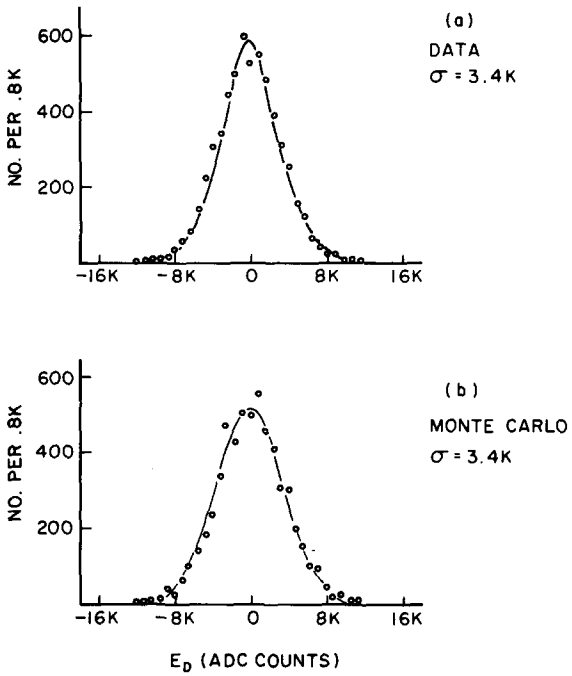

Fig. 5. Sampling fluctuations in 4 GeV electron showers ($\theta = 0°$), as observed in the data (a) and Monte Carlo simulation (b). Smooth curves are Gaussian distribution with $\sigma = 3400$ ADC counts.

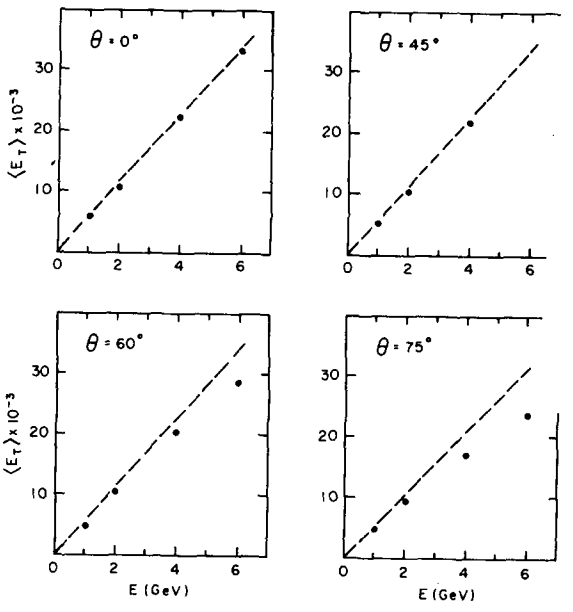

Fig. 6. Mean total pulse height as a function of electron beam energy for four angles of incidence. The dashed curves represent the calculated results for fully contained showers (see text). The slopes of the calculated curves are: 6270/GeV ($\theta = 0°$, 45°, 60°), 5500/GeV ($\theta = 75°$).

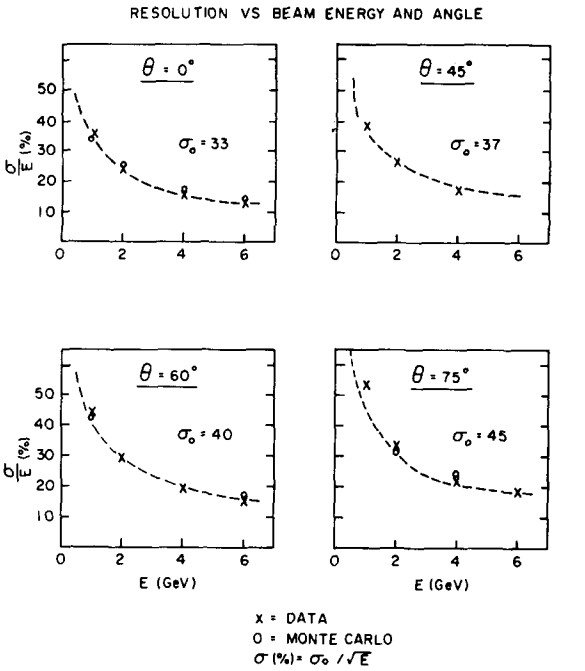

Fig. 7. R.m.s. energy resolution (percent) as a function of electron beam energy for four angles of incidence. The crosses are measured points; the circles are Monte Carlo calculations. The dashed curves are given by $\sigma(\%) = \sigma_0/\sqrt{E}\,(\mathrm{GeV})$, for the indicated values of σ_0.

(GeV) and angle θ (rad) is accurately parameterized as

$$\sigma(\theta, E) = 0.33\left[E(1+0.45\theta^2)\right]^{1/2}. \quad (2)$$

This relation is valid for angles up to 75°. For larger angles the response of the calorimeter becomes sensitive to the position of the beam entering the calorimeter relative to the nearest sampling channel.

It is noteworthy that the response, $\langle E_T \rangle$, of the calorimeter for a given energy (and for full shower containment) is independent of the angle θ up to $\theta = 60°$, and that at 75° the total pulse height differs from its value at 0° by only 7%. This is a matter of considerable practical importance for a detector covering large solid angles. In first approximation we expect at most a small variation with θ since (referring to fig. 2a) the projected

Table 1
Angular dependence of r.m.s. resolution width $\sigma(\theta, E) = \sigma_0(\theta)\sqrt{E}$

θ	$\sigma_0(\theta)$
0°	0.33±0.01
30°	0.35±0.02
45°	0.37±0.02
60°	0.40±0.03
75°	0.45±0.03

shower length along the calorimeter axis, and hence the number of wires struck, varies in inverse proportion to the thickness of gas along the shower direction. This compensation cannot be exact, especially at large angles, because of end effects due to finite absorber thickness between gaps and the fact that the path length of soft shower electrons through a sampling gap is only loosely coupled to the angle of incidence of the shower. Nonetheless as a practical matter it holds very well. Fig. 8, using Monte Carlo results for 4 GeV showers, shows the decrease in the mean number of sampled primary electrons (N_c) with increasing θ, while the total path length of electrons traversing the gaps (L_c) remains virtually constant. The signal is proportional to L_c.

These observations provide some insight into the mechanism for the angular dependence of the resolution width. We expect that the major contributions to the resolution width are Landau fluctuations in the energy deposited in the sampling gas and fluctuations in the number of sampled primary shower electrons. (A detailed discussion is given in sect. 4 below.) Since the total path length of primary shower electrons through the sampling gas is essentially independent of the angle θ, the Landau fluctuations do not play a role in the broadening of the resolution with increasing angle. The angular dependence of the resolution is governed by the decrease in primary shower statistics with increasing θ. Indeed, the θ-dependence given in eq. (2) follows directly from the calculated results for $N_c(\theta)$ shown in fig. 8a.

We have not made measurements of the resolution for angles in the x–z plane. We expect that the resolution for a given angle in the x–z plane is better than for the same angle in the y–z plane since the number of sampling gaps seen by the shower, per unit distance along z, increases with angle in this plane; hence, the decrease in sampling statistics is less pronounced. This expectation is borne out by the Monte Carlo calculations described in sect. 4.

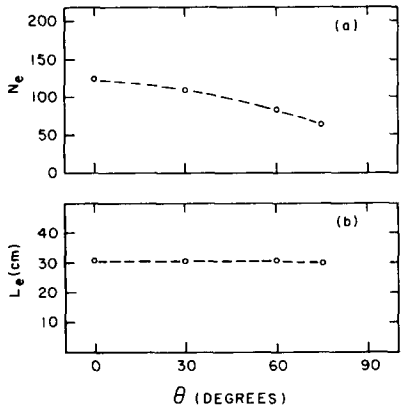

Fig. 8. The calculated mean number of sampled shower electrons (a), and the mean total path length in sampling gas (b) for 4 GeV showers as a function of θ.

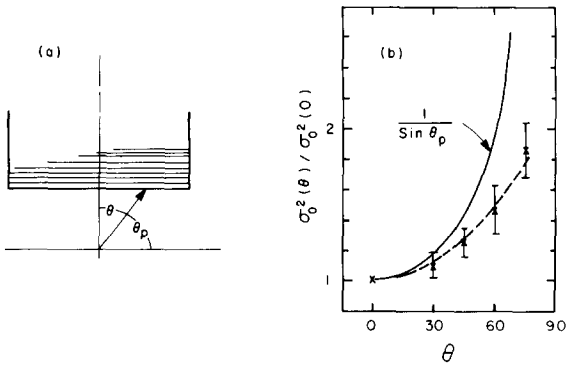

Fig. 9. (a) A possible geometry with the sampling wires aligned parallel to the beam direction, with scattering angle θ_p. (b) The measured increase of the resolution width with angle θ. The dashed curve is given by eq. (2).

The fact that the resolution function is well behaved even at very large values of θ is of importance for possible colliding beam applications in which the sampling channels lie parallel to the incident beams, as illustrated in fig. 9a, where $\theta_p = 90° - \theta$ is the polar angle for interactions. In this case, for a fixed transverse momentum (p_T) the momenta to be measured in the calorimeter go as $1/\sin\theta_p$, and this increases faster than σ^2 for a fixed p_T (fig. 9b). Thus, the relative measurement accuracy, which is proportional to $(\sigma^2/p)^{1/2}$, actually improves in the forward directions.

4. Other geometries: calculated results

The agreement between the measured and the calculated results for electron showers in our test module, as described above, appears good enough to allow reliable predictions over a range of sampling configurations for this type of calorimeter. In particular, as noted at the outset of this paper, the test module was designed to have minimal sampling volume with the aim of optimizing the flux carrying properties of a structure incorporated in magnet pole tips. This was done with some sacrifice in energy resolution for electromagnetic (but not hadronic) showers. It is of interest to see how the performance varies as this requirement is relaxed (i.e. for increased ratios of sampling volume to absorber volume). Also, we have noted that the 2×5 cross sectional aspect ratio of the sampling elements in our test module has given charge-collection problems which are best avoided in a practical detector, leading to a desire to investigate geometries in which this ratio is more nearly square.

In this section we present some results based on the Monte Carlo model for a class of calorimeter structures, similar to that of the test module, in which we vary the size and number of sampling channels for a fixed detector volume. (No saturation effects are incorporated in the results which follows.)

First, it is instructive to examine the origin of sampling fluctuations for calorimeters in which the sampling medium is a gas at atmospheric pressure. In fig. 10 we illustrate the calculated contributions to the energy resolution, comparing a "conventional" geometry of lead plates and MWPC planes with the high density geometry of the test device. In each case the lowest of the three curves corresponds to fluctuations in the number of sampled shower electrons, the next curve incorporates the variation in track length of shower electrons passing through the sampling volume, and the top curve gives the net resolution including Landau fluctuations in the energy loss. The "conventional" structure illustrated here, with $\sim 80\%$ of its volume in the MWPC planes, gives quite good resolution for a gas sampling calorimeter: The r.m.s. fluctuations in the number of sampled shower electrons amount to only $7\%/\sqrt{E}$. The resolution is dominated by path length and Landau fluctuations, and this is the reason for the generally poorer energy resolution obtained with proportional wire calorimeters in comparison with calorimeters of denser sampling media. As pointed out by Fischer [3] the effect of path length fluctuations is comparable, in the conventional structure, to that of the Landau fluctuations. For the high density calorimeter, as seen in the lower portion of fig. 10, the sparse sampling volume gives a resolution width dominated by shower electron statistics and Landau fluctuations. Fluctuations in path length give a negligible contribution here, and this is to some extent due to the limitation on track length variations imposed by the small dimensions (in x and z) of the individual sampling channels.

To examine some general features of high density devices we have computed the response for a class of calorimeter structures with the geometry illustrated in fig. 11, and the following specifications:

1) The absorber material is iron.

2) The sampling medium is argon gas at atmospheric pressure. The calculated signal is the total number of ionization electrons produced in the gas (no saturation).

3) The sampling channels are square in cross section.

4) The pattern of sampling channels is such that a line through the calorimeter parallel to the z-axis strikes one and only one sampling channel in each pair of successive sampling layers.

For this configuration the ratio of sampling volume to total volume is given by (referring to fig. 11):

$$R = b/2a. \qquad (3)$$

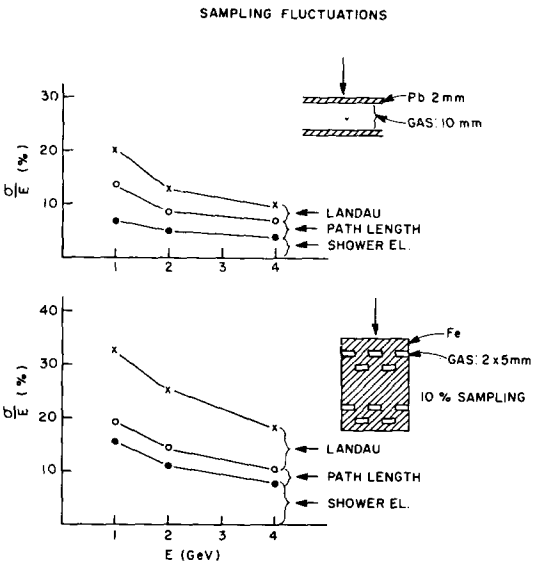

Fig. 10. Calculated contributions to the resolution width, comparing a conventional sampling geometry (top) with the tested geometry (bottom).

The pattern was chosen in order to investigate the trends of performance as the sampling ratio, R, and the width of the sampling channels, b, are varied. We do not claim that it is superior to other possible configurations in practical applications.

Fig. 12a shows the contributions to the energy resolution for 5×5 mm^2 sampling channels, as a function of the sampling ratio R. The calculations are for electron showers incident parallel to the z-axis ($\theta = 0$). The net resolution improves roughly as $R^{-1/2}$. It is interesting to note that for 50% sampling ($R = 0.5$) the resolution for this calorimeter is equal to that of the lead-MWPC geometry shown in fig. 10, although the relative contributions from shower statistics, path length and Landau fluctuations are different for the two cases. The mean absorber thickness between sampling channels

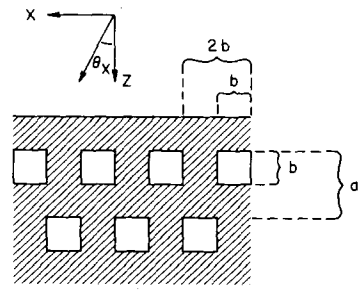

Fig. 11. Sampling geometry for the general class of structures described in the text.

(along the z direction) for the high density calorimeter is

$$t = b[(1/R) - 1]. \quad (4)$$

For $R = 50\%$ and $b = 5$ mm this gives $t = 0.3$ radiation lengths in iron, which is roughly equivalent to the 2 mm lead plates of the conventional calorimeter shown in fig. 10. From eq. (4) we see that the approximate $R^{-1/2}$ dependence of the resolution is analogous to the general observation that the resolution of sampling calorimeters goes as $\sqrt{t}$, where t is the incremental absorber thickness. This same trend is seen in fig. 12b, which shows the resolution for fixed density ($R = 0.25$) as a function of b, the sampling channel dimension. The resolution width increases as $\sqrt{b}$ for $b \gtrsim 2$ mm.

In fig. 13 we show the response as a function of the angle of the incident beam for the case $R = 0.25$, $b = 0.5$ cm: θ_x corresponds to inclination in the x–z plane, θ_y to inclination in the y–z plane. In both cases the total signal is insensitive to the angle, as was observed in the measurements made with test calorimeter (sec. 3). The increase in resolution width with the angle θ_y is nearly identical to that observed in the test beam measurements, with $\sigma(\theta_y)/\sigma(0) \simeq \sqrt{1 + 0.45\theta_y^2}$ [cf. eq. (2)]. The increase with θ_x is less pronounced, as expected on the basis of arguments given in sect. 3.

The results of calculations for the calorimeter geometry of fig. 11 can be summarized as follows (b in cm, θ in rad):

$$\sigma(\theta = 0) \simeq 0.22\sqrt{[b(1/R - 1)E]}, \quad (5a)$$

$$\sigma(\theta_x) \simeq \sigma(\theta = 0)\sqrt{(1 + 0.12\theta_x^2)}, \quad (5b)$$

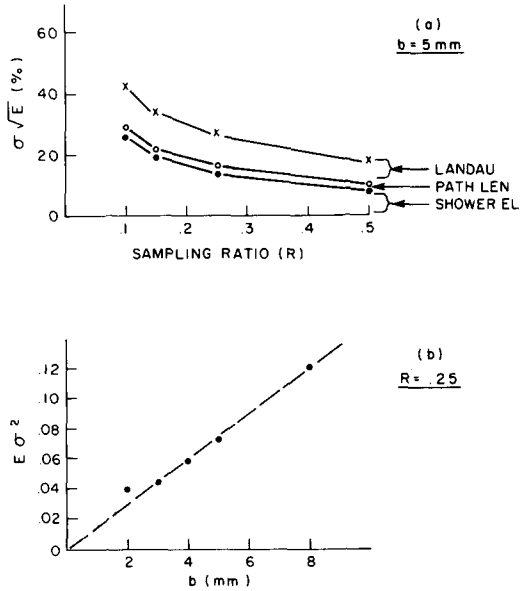

Fig. 12. Energy resolution for $\theta_x = \theta_y = 0°$: (a) As a function of the sampling ratio, R, for $b = 5$ mm. (b) As a function slot size, b, for $R = 0.25$.

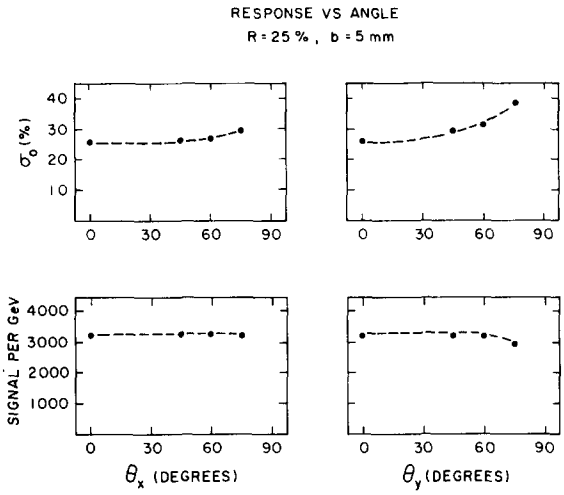

Fig. 13. Calculated response as a function of θ_x and θ_y for the geometry given by $R = 0.25$, $b = 5$ mm.

$$\sigma(\theta_y) \simeq \sigma(\theta = 0)\sqrt{(1 + 0.45\theta_y^2)}. \quad (5c)$$

These formulas give a good representation of the calculated response for the following range of parameters:

$0.2 \text{ cm} < b < 0.8 \text{ cm}$; $0.1 < R < 0.5$; $0 < \theta < 75°$.

A more precise parameterization would not be justified without more test data with which to confront the accuracy of the model..

5. Summary

We have measured the response to electron beams of a slotted iron calorimeter structure with gas proportional sampling and a gas-to-total volume ratio of 10%. The device is found to give usable energy resolution for incident beam angles up to 75° away from normal incidence, and the pulse height for fixed beam energy is flat over this range of angles.

The measured results are in good agreement with a Monte Carlo simulation developed to study the performance of gas sampling calorimeters. The calculation is based on the EGS shower routine [2], with a detailed accounting of ionization loss as shower electrons traverse the sampling gas [3]. This Monte Carlo program has been employed to investigate the origin of the observed sampling fluctuations and to parameterize the performance as a function of the number and size of sampling channels for a class of calorimeters similar in structure to the test device.

We thank the staff of the Brookhaven AGS for assistance and technical support in the test beam mea-

surements. In carrying out these studies we have profited from numerous insights gained in discussions with members of the R806/R807 experimental group at CERN, and the Instrumentation Division at BNL. We are indebted to H.G. Fischer for assistance in setting up the Monte Carlo calculation.

References

[1] T. Ludlam et al., IEEE Trans. Nucl. Sci. NS-28 (1981) 517.
[2] R.L. Ford and W.R. Nelson, SLAC-210 (1978).
[3] H.G. Fischer, Nucl. Instr. and Meth. 156 (1978) 81.